The Orbital and Spatial Distribution of the Kuiper Belt

JJ Kavelaars
Herzberg Institute of Astrophysics

Lynne Jones
University of Washington

Brett Gladman
University of British Columbia

Joel Wm. Parker
Southwest Research Institute

Jean-Marc Petit
Observatoire de Besançon

Models of the evolution of Neptune's migration and the dynamical processes at work during the formation of the outer solar system can be constrained by measuring the orbital distribution of the remnant planetesimals in the Kuiper belt. Determining the true orbit distribution is not simple because the detection and tracking of Kuiper belt objects (KBOs) is a highly biased process. In this chapter we examine the various biases that are present in any survey of the Kuiper belt. We then present observational and analysis strategies that can help to minimize the effects of these biases on the inferred orbital distributions. We find that material currently classified as the classical Kuiper belt is well represented by two subpopulations: a high-inclination component that spans and uniformly fills the stable phase space between 30 and 47 AU combined with a low-inclination, low-eccentricity population enhancement between 42 and 45 AU. The low-i, low-e component may be that which has long been called the "Kuiper belt." We also find weaker evidence that the high-i component of the classical Kuiper belt may extend beyond the 2:1 mean-motion resonance with Neptune. The scattering/detached disk appears to extend to larger semimajor axis with no evidence for a falloff steeper than r^{-1}. This population is likely at least as large as the classical Kuiper belt population and has an i/e distribution much like that of the hot classical Kuiper belt. We also find that the fraction of objects in the 3:2 resonance is likely around 20% and previous estimates that place this population at ~5% are inconsistent with present observations. Additionally, high-order mean-motion resonances play a substantial role in the structure of the Kuiper belt.

1. OVERVIEW OF THE HISTORY OF KUIPER BELT SURVEYS

In 1949 K. Edgeworth, and in 1951 G. Kuiper, postulated the existence of a debris disk beyond the orbit of Neptune based on the hypothesis that material in this zone had likely not formed into large planets (*Irwin et al.,* 1995). The 1930 discovery of Pluto (*Tombaugh,* 1961) was the result of a search for an object that would explain the (incorrectly) measured motions of Neptune. Although, at the time, Pluto was not recognized as a large member of an ensemble of material, many researchers recognized that a search of the outer solar system could prove fruitful (see chapter by Davies et al. for a thorough historical review). In particular, a measure of the mass and orbital distribution of material in this zone of the solar system could explain the source of short-period comets.

Initial surveys of the Kuiper belt were conducted with the assumption that objects discovered beyond Pluto would be undisturbed, pristine relics of planet formation. Dynamically cold, circular, and low-inclination orbits were expected. The first two Kuiper belt objects discovered after Pluto, 1993 QB_1 (*Jewitt et al.,* 1992) and 1993 FW (*Luu et al.,* 1993), fit the expectation. These discoveries were followed by the discovery of objects at distances of just ~35 AU, much closer than 1992 QB_1 or 1993 FW. Initially the astrometric positions of these new objects [1993 RO (*Jewitt et al.,* 1993), 1993 RP (*Liller,* 1993), and 1993 SB

and 1993 SC (*Williams et al.,* 1993)] were fit with orbits assumed to be circular (a necessary constraint due to the short discovery arcs available).

In *IAU Circular 5869,* Williams et al. noted ". . . there is rapidly developing a very severe problem of securing adequate astrometric follow-up, which is absolutely essential for any understanding of this exciting development in the outer solar system" (*Williams et al.,* 1993).

Soon after discovery, however, followup observations of 1993 SC were reported to the Minor Planet Center by *Tholen et al.* (1994) and demonstrated that the measured positions were better matched by a Pluto-like orbit with eccentricity of ~0.2. As a result of these observations the orbits of 1993 RO, 1993 RP, and 1992 SB were also assumed to be Pluto-like and new ephemerides were computed. At this time, B. Marsden released the following statement in *IAU Circular 5985*: "If the true orbits differ significantly from those on IAUC 5983, the ephemerides could be substantially in error . . ." (*Marsden,* 1994).

Even with these early warnings the avalanche of Kuiper belt object (KBO) discoveries quickly overwhelmed the followup efforts available, creating a distorted view based on ephemeris bias (defined below). Selection effects such as those described below also influenced the theoretical view of the Kuiper belt that has resulted from these surveys. *Jewitt et al.* (1996) provided one of the first attempts to quantify the size and shape of the Kuiper belt. In this early work they considered the biases against detections of high-inclination objects and determined that the intrinsic width of the Kuiper belt is likely around ~30° FWHM, much broader than anticipated. As surveys of the Kuiper belt have continued, observers are becoming more aware that a correct assessment of all observational bias is critical if one is to correctly measure the distribution of material in the distant solar system.

2. BIASES IN THE OBSERVED ORBIT DISTRIBUTION

2.1. Flux Bias

The most obvious bias in any optical imaging survey is "flux bias": Objects that are brighter are easier to detect and thus make up a disproportionate fraction of the detected population. Kuiper belt objects are discovered in the optical via reflected solar light, thus

$$\text{flux} \propto \frac{D^2}{\Delta^2 R^2} \qquad (1)$$

where D is the object's diameter, Δ is the distance between Earth and the KBO, and R is the distance between the Sun and the KBO ($R \approx \Delta$). This results in objects at 30 AU being ~8× (or 2.3 mag) brighter than the same-sized objects at 50 AU. In addition, an object with a diameter of 1000 km is ~100× (or 5 mag) brighter than a 100-km-diameter object, even if there is no difference in albedo between them. Determining the true population of the Kuiper belt requires accurate knowledge of the flux limits of the survey.

A result of this flux bias is that Plutinos are a large fraction of the observed population, as they can spend some fraction of their orbit interior to Neptune, making them easier to detect than an object on a circular orbit beyond 40 AU.

The immediate impact is that there is nearly no solid information about the population of small ($D < 10$ km) objects and only limited knowledge of the distant ($\Delta > 50$ AU) KBO population.

2.2. Pointing Bias

A second bias depends on the ecliptic latitude and longitude of the survey; each region of the sky will contain a different fraction of each orbital class than another region.

Most obviously, a survey of fields near ecliptic latitude 10° will not detect any objects with inclination below this value, regardless of the fraction of objects with low inclinations. On the other hand, conducting a survey directly in the ecliptic plane is more efficient at detecting low-i than high-i objects. Objects with higher inclinations, which spend only a small fraction of their orbits near the ecliptic plane, will be poorly represented in an "on ecliptic" survey (see Fig. 11 in *Trujillo et al.,* 2001b). With typical KBO sample sizes of a few hundred objects at most, this results in poor statistical sampling of high-i KBOs.

Furthermore, Plutinos come to pericenter at solar longitudes that are far from Neptune and anti-Neptune. Thus, a flux-limited survey will be more sensitive to nearby objects and detect a higher fraction of Plutinos (vs. classical KBOs) when observing near quadrature with Neptune than when observing near Neptune or anti-Neptune, where the Plutinos are near aphelion. More generally, each mean-motion resonance has specific longitude ranges (relative to Neptune) where objects come to perihelion.

Knowledge of the pointing history of a survey must be available if one hopes to disentangle the true underlying population of the Kuiper belt from the biased observed one.

2.3. Ephemeris Bias

Ephemeris bias is particularly insidious. During a nominal survey of solar system objects, the initial discovery observation provides a first estimate of the orbit of the body. For objects in the asteroid belt, an observational arc of a week is sufficient to provide a reasonably robust measure of the asteroid's orbit, such that the object can be found again at some later date.

For the Kuiper belt, an arc of a few days does little more than to estimate the current distance and the orbital inclination of the object to within ~10–30%. Beyond these first-order measures, little orbital information is available. To predict the location of the object at a later date, strong orbital assumptions must be made, the most common being to assume that the object is on a circular orbit. The assumption made is almost certainly incorrect but does allow a first

order estimate of the location of the object (accurate to ~60") a few months after discovery. If, however, the newly discovered KBO is not observed again within a few months of discovery, then only those objects for which the orbital assumptions are correct will be recovered one year later. Unfortunately, those objects for which incorrect assumptions are made will be lost and the part of the orbit parameter space they represented may be lost with them (see Fig. 1).

Directed followup more than a few months after initial discovery tends to cause surveys to "leak" those objects that are most likely to have been indicating some new part of parameter space. Ephemeris bias keeps the orbit distribution looking like the assumed distribution that went into the ephemeris estimate, which may not look anything like the underlying orbit distribution.

2.4. Detection Bias

Observational surveys for KBOs proceed via comparing images (i.e., blinking), or comparing source catalogs constructed at different epochs. However, the sky density of asteroids in any given survey field is much higher than that of KBOs and so the time between epochs is kept short enough (~1 h) that asteroid confusion is minimized. Kuiper belt objects at 75 AU only move at ~2"/h; in a typical survey they will move only two seeing disks between epochs. More distant objects have even smaller sky motions and their detection is even more problematic. Combining the difficulty in aligning images with the image quality of typical groundbased large-area surveys, it is little wonder that objects beyond 75 AU are found so rarely. A careful examination of detection efficiency as a function of source distance must be conducted in order to determine the true radial limit of a survey.

Given the flux, pointing, ephemeris, and detection biases, it is little wonder that 500-km-diameter objects on high-inclination orbits with pericenters outside 50 AU are seldom detected.

2.5. Survey Design

Completely removing all observer biases from a given survey is impossible. Flux, pointing, and detection biases reflect the intrinsic problem of observing solar system objects and cannot be eliminated by clever observing strategy. Ephemeris bias, however, can be greatly reduced by a carefully planned observing program.

Ephemeris bias is maximized when observers rely completely on ephemeris predictions based on poorly constrained orbits. For KBOs the uncertainty in the ephemeris based on observational arcs of only a few hours to days exceed the field of view (~10 arcmin) of most facilities where recovery observations are attempted in the following opposition (see Fig. 1). Although this problem was realized quite early in Kuiper belt surveys, the insidious nature of the bias ensured that the full impact could not be realized because "you don't know what you're missing."

A straightforward approach to eliminating ephemeris bias is, simply, to follow the targets more frequently during the discovery opposition and to avoid targeted followup observations in favor of repeatedly observing the same large area of sky. The slow motion of KBOs ensures that they can be reobserved within a few degrees of their discovery location over the course of many months and even years. Thus, a survey that worked in patches larger than a few square degrees could repeatedly image the patches in order to obtain "serendipitous" followup that would then be free of ephemeris bias. This notion of blind followup is precisely what has been employed by the Canada-France-Ecliptic Plane Survey (CFEPS) (*Jones et al.,* 2006) and is the planned strategy for surveys to be run by the LSST and Pan-Starrs projects.

Reliable ephemeris predictions, which ensure successful pointed recovery of a given object, are achievable once the object has been tracked through the second apparition using a frequent followup strategy. Figure 2 presents the evolution of the orbital and ephemeris uncertainty for an object tracked by CFEPS. This figure demonstrates the rapid growth in the ephemeris uncertainty and indicates that, without a ~6–8-week arc of observation in the discovery opposition, an object ephemeris uncertainty is >2000 arcsec. Additionally, until observations in the third opposition are available, precise classification is not feasible.

3. DEBIASING THE SURVEYS

The past decade and a half has seen a large number of surveys of KBOs. Initially these surveys focused on the detection of objects, proving the existence of the Kuiper belt. During this initial "discovery" phase, any new detection provided new insight into structure of the Kuiper belt. The discovery of 1992 QB_1 proved the existence of the Kuiper belt. The realization that there are a large number of objects in 2:3 resonance with Neptune made clear the importance of resonances. The subsequent discovery of 1999 TL_{66} (*Luu et al.,* 1997) and other objects on "scattering" orbits introduced a further complication to the dynamics of this region (*Duncan and Levison,* 1997). The existence of "detached" objects (*Gladman et al.,* 2002) on a variety of large-a and large-pericenter orbits, such as 2000 CR_{105} (*Elliot et al.,* 2005), Sedna (*Brown et al.,* 2004), Eris (*Brown et al.,* 2005), and 2004 XR_{190} (aka Buffy) (*Allen et al.,* 2006), is further challenging models of the formation of the Kuiper belt.

Table 1 lists Kuiper belt surveys that are currently in the literature along with the basic parameters of each survey. Some of the surveys listed in Table 1 are ongoing and quantities listed in the table provide a snapshot of the current detection statistics.

With these discoveries also come questions: What is the total population of the material in the "Kuiper belt"? What fraction of the population is in resonance? How can these objects come into resonance? What is the relative size of the "scattered" component? How stable is this component? How large a population do objects like 2001 CR_{105} and

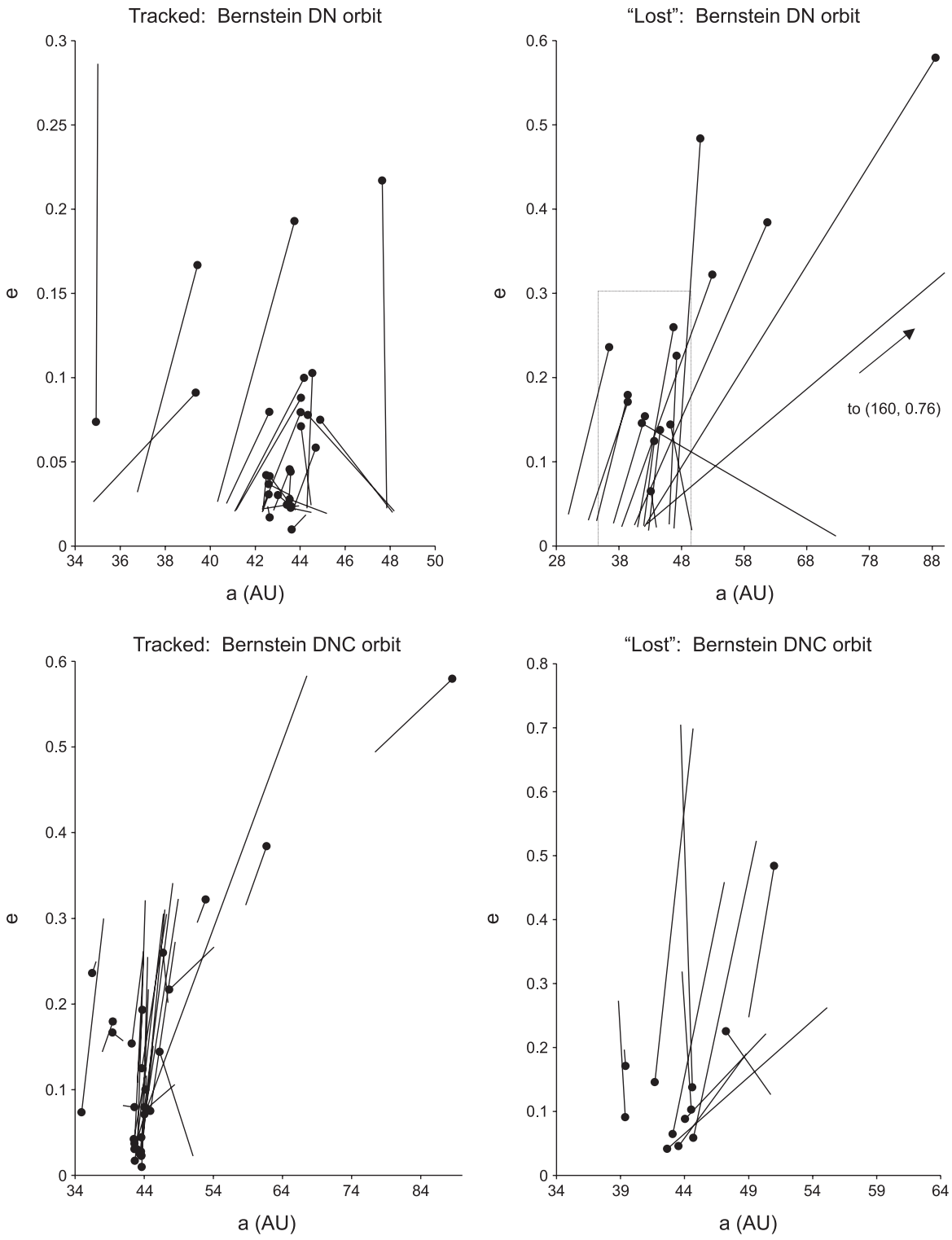

Fig. 1. An indication of the effects of ephemeris biases. The top left panel shows the a/e change from discovery-arc-based orbits (start of lines) to final orbits based on multi-opposition tracking (points at end of line) for the CFEPS "L3" release. The right panel presents the same information for those CFEPS L3 objects that, one year after discovery, were more than 10 arcmin from the ephemeris based on their discovery-arc orbits. Those objects in the right panel would have been "lost" by recovery attempts at telescopes with FOVs of 10 arcmin or less. The figure demonstrates that those objects whose orbits are outside the classical belt region are more likely to be lost, due to ephemeris bias. The bottom set of panels demonstrates that the loss rate is much lower when a 60-d arc in the discovery opposition is available before small FOV recovery is attempted.

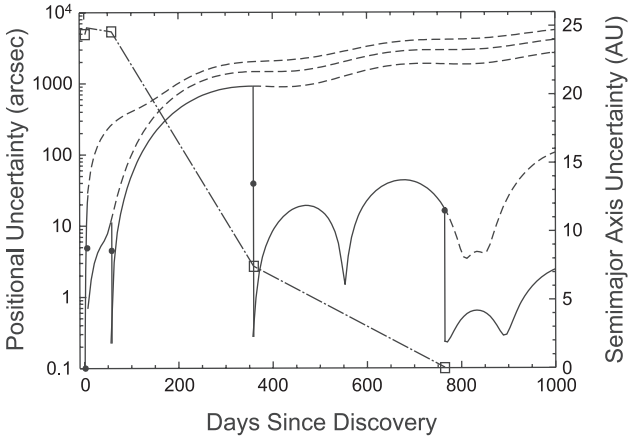

Fig. 2. Time evolution of positional and semimajor axis uncertainty for a classical-belt object. The solid line indicates the evolution of the predicted ephemeris uncertainties (based on orbfit from *Bernstein and Khushalani,* 2000) as additional observations are acquired; solid dots indicate the observed ephemeris error at each recovery. The dashed lines indicate the ephemeris uncertainty growth without the additional observations at each epoch. The dash-dot lines indicate the semimajor axis uncertainty as additional observations are acquired. Clearly tracking with a large (>10') field of view facility is required for the second opposition recovery observations. The semimajor axis uncertainty is too large for classification until after recovery observations in the third opposition.

Sedna represent? How did they come to be in their current orbits? What fraction of objects are like 2004 XR_{190}? Is there a vast reserve of distant large bodies like Eris? Clearly surveys of this region of the solar system continue to provide challenging observations.

3.1. Analytical Approaches to Debiasing

The sources of biases introduced into the observed representation of the underlying Kuiper belt are all well understood (see previous section), making the bulk properties of the underlying population determinable based on the analytic modeling of these biases. Such analytic modeling approaches can even be useful for deriving bulk information from surveys with little to no characterization information available.

3.1.1. The inclination distribution. Unfortunately, one cannot invert the observed inclination distribution and from that determine the intrinsic distribution function. *Jewitt et al.* (1996) first noted that the inclination distribution of material in the Kuiper belt must be quite broad. This conclusion was based on their detection of a number of high-inclination (>10°) KBOs even though their survey was confined to be near the plane of the ecliptic. Jewitt et al. found that either a "box" distribution [i.e., N(i) ~ *constant*] or a single broad Gaussian provided reasonable representations of this

TABLE 1. List of Kuiper belt surveys.

Survey	Facility	Area	Depth	Secure	Detections	Reference
Irregular Sat.	CFHT/12K	11.85	24.0	0	66	*Petit et al.* (2006a)
DES	KPNO/CTIO	550	22.0	217	486	*Elliot et al.* (2005)
ACS	HST	0.02	28.3	0	3	*Bernstein et al.* (2004)
Caltech	Pal 0.6 m	19389	20.5	54	71	*Trujillo and Brown* (2003)*
Allen1	KPNO	1.5	25.5	6	24	*Allen et al.* (2001)
Allen2	CTIO	1.4	24.8	0	10	*Allen et al.* (2002)
SSDS	Sloan	100	21.5	0	1	*Ivezić et al.* (2001)
KPNO-Large	KPNO0.9/Mosaic	164	21.1	4	4	*Trujillo et al.* (2001a)
CFH/12	CFHT 3.6	0.31	25.93	2	17	*Gladman et al.* (2001)
CFHT	CFHT 3.6	73	23.7	59	86	*Trujillo et al.* (2001b)
Spacewatch	KPNO 0.9 m	1483.5	21.5	36	39	*Larsen et al.* (2001)
sKBO	CFHT/12K	20.2	23.6	0	3	*Trujillo et al.* (2000)
sKBO	UH2.2/8K	51.5	22.5	0	1	*Trujillo et al.* (2000)
Baker-Nunn	APT-0.5 m	1428	18.8	1	1	*Sheppard et al.* (2000)
CB99	KECK/LRIS	0.01	27.0	0	2	*Chiang and Brown* (1999)
SSO	Siding Spring	12	21.0	0	1	*Brown and Webster* (1998)
JL Deep	Keck	0.3	26.3	1	6	*Luu and Jewitt* (1998)
G98a	CFHT/UH8k	0.35	24.6	1	1	*Gladman et al.* (1998)
G98b	Pal 5 m	0.049	25.6	1	4	*Gladman et al.* (1998)
G98c	Pal 5 m	0.075	25.0	0	0	*Gladman et al.* (1998)
JLT	CFHT/UH8k	51.5	23.4	12	13	*Jewitt et al.* (1998)
Pluto-Express	CFH12K	2.2	23.5	3	4	*Trujillo and Jewitt* (1998)
MKCT	UH2.2 m	3.9	24.2	10	14	*Jewitt et al.* (1996)
MKCT	CTIO 1.5 m	4.4	23.2	1	3	*Jewitt et al.* (1996)
ITZ	WHT	0.7	23.5	2	2	*Irwin et al.* (1995)

*See also the chapter by Brown.

very early dataset. *Brown* (2001) developed a procedure that allows the comparison of analytical models and observations of the inclination distribution of KBOs. Brown suggested, based on an examination of the observed inclination distribution, that a reasonable analytical approximation for the inclination distribution is a superposition of two Gaussian distributions such that the intrinsic inclination distribution has the form

$$f_t = \sin(i)\left[a e^{-\frac{i^2}{2\sigma_1^2}} + (1-a) e^{-\frac{i^2}{2\sigma_2^2}} \right] \quad (2)$$

and the observed ecliptic distribution takes the form $f_e(i) = f_t(i)/\sin(i)$ (see *Brown,* 2001).

We use this same approach to examine the inclination distribution of different KBO subpopulations using the classification list compiled in the chapter by Gladman et al. (see Table 2).

We find that equation (2) provides a reasonable representation of the inclinations distributions for the four subpopulations of the belt examined (see Table 2). However, as previously found in *Brown* (2001), the range of parametric values allowed for the scattering, detached, and Plutino populations are all consistent with a nonexistent "low-inclination" component. Using a similar approach to debiasing their survey, although more carefully tuned to their observations, *Elliot et al.* (2005) match three different model distributions to their observed inclination distribution. They find that the global KBO population is best represented as either a double Gaussian (equation (2)) or as a single narrow Gaussian plus a broad Lorentzian. The main conclusion from their analysis is that the bulk inclination distribution is double peaked. They conclude, however, that the narrow-inclination component is dominated by the classical belt population and find that the "scattered" disk objects show little concentration toward low inclinations.

In effect, the double-Gaussian fit to the classical population tells us that a low-inclination (cold) component must exist for this subpopulation of the Kuiper belt. The other components of the belt, however, are well represented as having just a high-inclination (hot) component with a Gaussian width that is similar to the "hot" component of the classical Kuiper belt.

TABLE 2. Parametric representation of the inclination distribution of various subpopulations of the Kuiper belt for the inclination model in equation (2).

Population	σ_1	σ_2	*	$D\sqrt{N}$
Classical	1.5 ± 0.4	13 ± 3	0.95 ± 0.02	0.56
Scattered	1.6 ± 1.6	13 ± 5	$0.4^{0.8}_{0.0}$	0.72
Detached	1.1 ± 0.4	18 ± 6	$0.8^{1.0}_{0.0}$	1.26
Plutinos	1.7 ± 0.4	13 ± 5	$0.4^{0.8}_{0.0}$	0.7

*Values of $D\sqrt{N} > 1.5$ rejected at the ~1σ level (see *Brown,* 2001). None of the $D\sqrt{N}$ values for the models fits reported here reject the underlying model distribution. The parameters determined in this work are consistent with those reported in *Brown* (2001).

3.1.2. The distance distribution. *Trujillo and Brown* (2001) established that the radial distribution of material in the Kuiper belt can be determined using the apparent radial distribution via the equation

$$f(R) = \frac{\beta(R) f_{app}(R)}{\Gamma'(m_V)} \qquad \beta \equiv \left[\frac{R^2 - R}{R_0^2 - R_0} \right]^{q-1} \quad (3)$$

where $f_{app}(R)$ is the observed (apparent) radial distribution, R_0 is the inner edge of the Kuiper belt (taken to be $R_0 \sim 42$ AU for the Kuiper belt as whole and $R_0 \sim 35$ AU for the scattering component when treated separately), $\beta(R)$ is the bias correction factor, and $\Gamma'(m_V)$ is the normalization constant, which depends only on the flux from the detected objects and does not affect the radial distribution (see *Trujillo and Brown,* 2001, for a complete derivation). Trujillo and Brown required that the following assumptions be met for their debiasing approach: (1) all KBOs follow the same size distribution, described by a differential power law; (2) observations are conducted at opposition allowing the transformation $\Delta = R - 1$; (3) the albedo is not a function of size or heliocentric distance R.

Evidence of a "break" in the luminosity function of KBOs has been detected (*Bernstein et al.,* 2004) [see also the chapter on the luminosity function (LF) by Petit et al.] and the albedos of KBOs are now recognized to have some dependence on object size (see chapter by Stansberry et al.). Even in light of these changes in circumstance, one can still use the above formalism, since the break in the LF is faintward of the majority of objects in the MPC database used in our analysis and albedo only appears to vary for the largest KBOs. Additionally, as shown in *Trujillo and Brown* (2001), the debiasing of the radial distribution is only weakly dependent on albedo.

Figure 3 presents the debiased radial distribution for three subsets of the classified KBOs with $H > 3.5$. The figure clearly demonstrates that the "cold classical" KBOs radial distribution is peaked near ~44 AU while the "hot classical" component of the population is more broadly distributed. Interestingly, the "hot" and "cold" components of the belt have identical radial distributions beyond ~46 AU. The scattering/detached KBOs exhibit more extended radial distributions with no obvious preferred distance.

The radial distribution of the classified populations has an unknown amount of ephemeris bias, since we don't know which objects from the originally detected population were lost due to being misclassified, nor if there was a strong distance/orbit correlation among those losses.

Although Fig. 3 provides a compelling picture of a truncated disk, the debiasing approach described by Trujillo and Brown is only effective in those parts of the solar system where we have actual detections, *unless we know a priori that the surveys present in the MPC were sensitive to objects beyond the apparent limit of the classical belt,* which seems likely to be true only out to distances of ~75 AU. Based on the available detections and this analytic debiasing approach, we conclude that the radial falloff of the classical

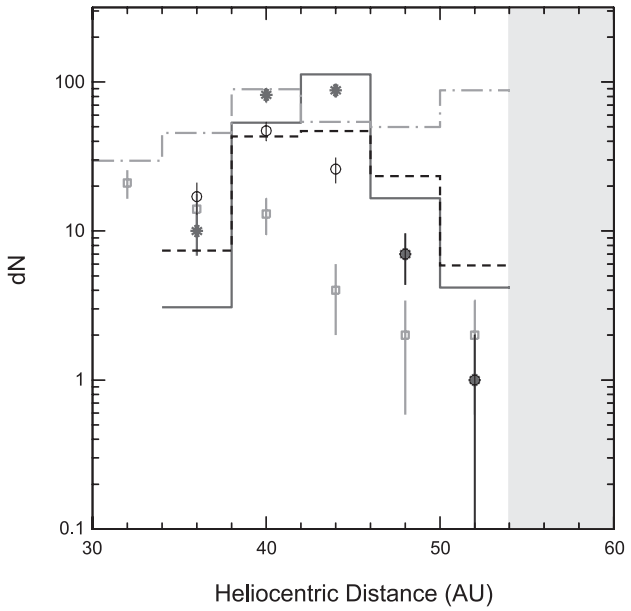

Fig. 3. The radial distribution at detection of classified KBOs with H > 3.5. The points represent the distribution of detected KBOs (asterisks: classical KBOs with inclinations <5°; black open circles: classical KBOs with inclinations >5°; gray boxes: scattering and detached KBOs). The lines (solid line: "cold" classical; black dashed: "hot" classical; gray dot-dashed: scattering/detached) represent the radial distribution after debiasing based on the method in *Trujillo and Brown* (2001). The "cold classical" belt object density must decay very rapidly with distance beyond ~45 AU; the "hot classical" appears less "peaked" than the "cold" classical component. Remarkably, the cold and hot radial distributions are identical beyond 45 AU, indicative of a single, underlying, population. The scattering/detached belt object density does not appear to be a strong function of distance. The shaded area of the plot represents that part of the solar system where no dynamically classified objects with H > 3.5 have been detected. Vertical scale indicates relative population at each distance.

belt must be quite steep and the "hot" classical belt objects extend inward to slightly lower heliocentric distances where their larger inclinations help ensure their stability. The scattering and detached objects do not appear to share this distribution.

3.2. Survey Simulator Debiasing

The complex interaction between the various biases outlined above and the orbital distribution results in a situation where detailed comparisons between model and observations cannot be achieved using analytic debiasing approaches. Like the construction of the models themselves, detailed comparison requires the use of a simulator. Essentially the survey simulator entails mapping the model space into the observation space. Such approaches have been detailed in some previous Kuiper belt surveys (see, e.g., *Jewitt et al.,* 1998; *Trujillo et al.,* 2001b; *Jones et al.,* 2006).

A survey simulator provides a programmatic method of introducing into the model those same biases that are present in the observational data. By correctly emulating the processes of surveying, a meaningful comparison can be achieved. For this method to be successful the user must look to as many constraining surveys as possible for testing their model orbital distribution.

We provide here a rough outline of the operation of the CFEPS survey simulator:

1. A randomly selected model particle is assigned a size, based on some externally calibrated understanding of the size distribution.
2. The sky location and brightness are determined based on the model particle's orbit.
3. The observability of the object is compared to the characterization of the survey and detected objects are kept.
4. The above steps are repeated until a sample with the same size as the survey is achieved,
5. The orbital elements of the simulated survey are compared to the observed Kuiper belt.
6. The model is tuned to better represent reality and the above steps are repeated.

When a model that provides a compatible simulation of the observations is found, this model can be accepted as a reasonable (although possibly not unique) representation of the true underlying population. Various bulk orbital properties and other details can be determined by examining the model distributions.

3.2.1. Survey characterization. A full and correct characterization of the survey's detection efficiency is critical to the successful use of a survey simulator approach. For each of the biases present in the survey, the information needed to model this bias must be determined from the survey observations. For each field of the survey the ecliptic longitude and latitude must be reported along with a determination of the flux-based detection efficiency as a function of the sky rate and angle of motion of KBOs in the field.

Providing the details required to allow accurate survey simulations is a great burden on the survey observer. Without this information, however, the modeler is left with only the rough analytic comparisons detailed above and determining the true underlying orbit distribution may never be possible.

3.2.2. Model uniqueness. A strong caveat must be made for both the analytic and survey simulator approaches to comparing model distribution with the observed population. A model, when convolved through a survey simulator, may look like the observed population, or the observed population when analytically debiased may resemble the model; however, this does not ensure any uniqueness of the model distribution. For an accurate picture to emerge modelers must produce a range of possible scenarios for the dynamical state of the belt and then through piecewise comparison various unfavorable scenarios can be eliminated with no guarantee that the true underlying population will ever be found.

Most of the survey simulator results come in the form of constraints that can be placed on those orbital elements that require longer observing periods before they can be determined accurately, such as a and e. In addition, survey simu-

lators are an excellent approach to determining the relative strengths of the various orbital populations. For each of the orbital distributions discussed in the analytic section, we present a short review of similar results that have been derived using survey simulator approaches.

We conclude each section by describing the results we obtain using the CFEPS survey simulator and the CFEPS L3 (*Petit et al.,* 2006b) and Pre-Survey (Jones et al. 2006) data releases. Figure 4 presents the a/e/i distributions for the CFEPS + Pre-Survey detections, our base model, and the "simulated detections." This model is discussed further in the following sections.

3.2.3. The inclination distribution. Based on early evidence of a broad (in latitude) Kuiper disk, *Trujillo et al.* (2001b) conducted observations at a variety of ecliptic latitudes and then, using their knowledge of the pointing history of the survey, matched the observed latitude density distribution to the underlying inclination distribution. They found that the latitude distribution of material in the Kuiper belt could be reproduced by assuming that the underlying inclination distribution followed the form of a single Gaussian of width $\sigma \sim 20°$. Trujillo et al. also found that the functional form in equation (2) or a simple "constant" distribution like that proposed in *Jewitt et al.* (1996) did an equally good job of matching their observations (an example of survey nonuniqueness). Inclination distributions that are nonzero at i = 0 while nonphysical appeared to provide a reasonable match to the data.

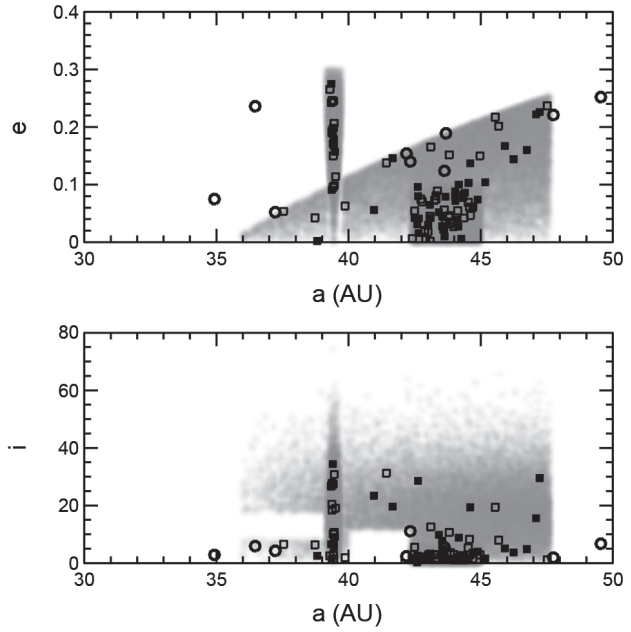

Fig. 4. The CFEPS L3 + Pre-Survey base model of the a/e distribution of material in the classical Kuiper belt plus the Plutino population (taken from *Kavelaars et al.,* 2006). Dots represent the model parent population, open squares represent the simulated observed population, filled squares are the orbital elements of the actual L3 + Pre-Survey detections, open circles represent the orbital parameters of L3 sources that were found to be in various Neptune mean-motion resonances and are not represented by the base model. The processes of "sampling" the base population through the survey simulator is highly stochastic and the sampling shown here is merely representative of one of many realizations performed to evaluate the validity of the model.

Based on the CFEPS survey simulator we find that the inclination distribution of the L3 + Pre-Survey sample, taken as a whole, is well represented by a either a double Gaussian, as in section 3.1.1, or by a flat inclination distribution modified by sin(i); this is very similar to the result found by *Jewitt et al.* (1996) and *Trujillo et al.* (2001b).

When we consider only those KBOs that are found to be part of the "classical" Kuiper belt between 40 < a < 47.5 AU, we find that models with only a single broad inclination distribution are rejected, much as found by *Elliot et al.* (2005) and *Brown* (2001) and in section 3.1.1. We conclude that *Jewitt et al.* (1996) and *Trujillo et al.* (2001b) did not require substructure in the inclination distribution because this structure is only present in the classical Kuiper belt populations.

Using the CFEPS survey simulator we explored the range of "double Gaussian" models allowed for the 40 < a < 47.5 AU zone and find that the results are basically identical to those found in section 3.1.1. Also, as determined via analytic debiasing in section 3.1.1, we find that there is no evidence of a double-component inclination distribution in the Plutino population.

3.2.4. The radial extent of the classical Kuiper belt. The initial explosion of discoveries of KBOs soon pointed to an apparent lack of objects on low-eccentricity orbits with semimajor axis beyond ~50 AU. Initial work on this problem by *Dones* (1997) indicated that, with only a handful of KBOs known at the time and the assumption of a flat luminosity function, a nonzero number of KBOs should have been detected with a > 50 AU if such objects existed. Further Monte Carlo or "survey simulator" analysis in *Jewitt et al.* (1998) indicated that a "classical" Kuiper belt smoothly extending to a > 50 AU was rejected by the available observations. A deep survey by *Gladman et al.* (2001) found a number of objects beyond the 50-AU limit, consistent with a model of radially decaying density. Since none of their detected KBOs beyond 50 AU were on circular orbits, Gladman et al. concluded that the lack of a population of KBOs on circular orbits beyond 50 AU was not inconsistent with their survey results. Further observational work by *Allen et al.* (2001) demonstrated that if the classical belt did extend beyond 50 AU, then the surface density in that region must be exceptionally low. Additional compelling evidence for an edge at ~50 AU has come from survey-simulator-style analysis from *Trujillo et al.* (2001b). More recently, *Hahn and Malhotra* (2005) attempted to construct a pseudo-survey-simulator analysis of the KBO orbits in the Minor Planet Center database, and they remarked that the lack of known KBOs on circular orbits with a > 50 appears to be consistent with a belt that is truncated at a ~ 45 AU.

Using our survey simulator approach we have found that the semimajor axis distribution in the zone between 40 and 47 AU cannot be modeled using a single functional form. We are forced to separate the semimajor axis distributions for the hot and cold components and discuss the radial extent of the Kuiper belt in this context.

3.2.5. The "hot" and "cold" classical Kuiper belt. Guided by the previous analytic and survey simulator efforts as well as plots of the a/e/i distribution of the classifiable KBOs (see chapter by Gladman et al.), we used the CFEPS survey simulator to examine the semimajor axis distribution of the nonresonant KBOs with $30 < a < 50$ AU and $e < 0.2$. Our best-fit model for the "cold" population has semimajor axis distributed between 42 and 45 AU with e uniformly distributed between 0 and 0.1. We also find that the semimajor axis distribution of the "cold" population (i.e., those objects with inclinations drawn from a Gaussian of width 1.5°) is inconsistent with a semimajor axis distribution that extends to $a > 45$ AU; the falloff in density is very steep beyond $a \sim 45$. We find the remarkable result that this low-inclination (cold) component appears to be tightly confined to a region between $42.5 < a < 44.5$ AU with eccentricities randomly distributed between 0 and 0.1. Those "classical" KBOs in the 42.5–44.5-AU zone with large inclinations, as well as all "classical" KBOs outside this narrow range of semimajor axis, appear to be drawn from a single high-inclination component with eccentricities drawn from a uniform phase-space distribution, $P(e) \propto e$. Based on these models, we find that ~35% of the "classical" Kuiper belt resides in a cold low-e/low-i component in the $42.5 < a <$ 44.5-AU zone, with the remaining ~65% in the "hot" component of the inclination/eccentricity distribution. Thus, we find that there is an enhancement of low-inclination orbits in the 42–45-AU region superposed on a uniform hot population covering all stable phase space from 30 to 47.5 AU and perhaps even to ~60 AU if the detached KBOs are considered to be the large-a extension of the "hot" classical belt.

3.2.6. The Plutino fraction. Nearly contemporaneously with the discovery of the first "Plutinos" *Malhotra* (1993) explained Pluto's "peculiar" orbit as being the result of a resonance trapping caused by the outward migration of Neptune. A mapping of structure and size of the Plutino population provides a strong constraint on this migration model.

Initial estimates of the fractional sizes of various subpopulations of the Kuiper belt were made in *Jewitt et al.* (1998), who reported on the detection of 13 KBOs in a survey of ~51 deg^2 and then compared them to the complete set of observed Kuiper belt objects with Monte Carlo realizations of various models of the belt populations. Using the ≃50 KBOs then known, Jewitt et al. found that 10–30% of the Kuiper belt is made up of 3:2 resonant objects; the lack of 2:1 resonators (at that time) was in mild conflict with models of Neptune's migration. However, Jewitt et al. cautioned that these conclusions were not firmly established by the available observations.

Trujillo et al. (2001b) determine a Plutino fraction by debiasing their detected population using a previously determined scaling relation (*Jewitt et al.,* 1998). *Trujillo et al.* (2001b) determined that the intrinsic ratio of Plutinos to classical belt objects is ~5%. The bias estimate in *Jewitt et al.* (1998), however, assumed that the Plutinos have an inclination distribution like that of the classical belt. In addition, Jewitt et al. had determined the bias fraction for the selection of fields that they observed, and the application of this same bias factor to the fields observed in *Trujillo et al.* (2001b) is not correct.

Hahn and Malhotra (2005) use their pseudo-survey-simulator approach to estimate the intrinsic Plutino fraction based on orbits in the Minor Planet Center database. They find that the observed Plutino fraction is quite low, near just 4% for the faintest Plutinos, and conclude that the intrinsic fraction is far below that predicted by resonance capture models alone.

Using the CFEPS L3 survey simulator we find that an eccentricity distribution of $P(e) \propto \exp((e - e_o)^2/\sigma_e)$ with a cut at $e > 0.3$ does a satisfactory job in reproducing the observed eccentricity distribution of the L3 + Pre-Survey sample when $e_o \sim 0.15$ and $\sigma_e \sim 0.1$. This eccentricity distribution, combined with an inclination distribution of a single component Gaussian ($P(i) \propto \sin(i) e^{-i^2/2\sigma^2}$) of width like that of the "hot" classical KBOs and a flat distribution of libration amplitudes between 0° and that of Pluto, does an excellent job of reproducing the L3 + Pre-Survey Plutino detections. Based on our Plutino model and comparing with our "hot" + "cold" Kuiper belt model, we find that the Plutino population is ~20 ± 10% the size of the "hot" + "cold" components of the classical Kuiper belt. This larger size for the Plutino population is much more consistent with models of migration of Neptune that normally result in very efficient capture into the 3:2 resonance and agrees well with estimates from *Jewitt et al.* (1998) but starkly contrasts the population estimates in *Trujillo et al.* (2001b) and *Hahn and Malhotra* (2005), who find that only a few percent of the intrinsic population is trapped in the 3:2 resonance with Neptune. We find that models with Plutino fractions as low as 4% are rejected at the 95% confidence level.

The *Trujillo et al.* (2001b) lower estimate of the Plutino fraction is on based their comparison of the entire population of objects they declared as Plutinos with the entire population of objects they declared as classical KBOs without recognizing that the latitude distribution of Plutinos is different from that of the low-inclination classical KBOs. The situation is further complicated: Of the seven objects that Trujillo et al. report as Plutinos, Gladman et al. (see chapter in this book) find that only five are robustly classifiable; two have been lost. Of the five classifiable Plutino candidates two, 1999 CP_{133} and 1999 RW_{215}, are in the 5:4 and 4:3 mean-motion resonance, not the 3:2 as determined from their discovery orbits, thus the sample has shrunk to just three Plutinos. Of the remaining three robustly classified Plutinos, one was found in the "high" ecliptic fields while

two classical KBOs were found in those fields. Thus, the observed Plutino fraction in these fields, where the latitude distribution of Plutinos and classical KBOs is more similar than on the ecliptic, is 50% the size of the "hot" classical population, thus the intrinsic Plutino fraction may be much higher than the estimated 5% value.

3.2.7. The 2:1 and other resonances. *Chiang et al.* (2003a,b), *Hahn and Malhotra* (2005), *Lykawka and Mukai* (2007), and the Gladman et al. chapter present methods of searching for the resonance characteristics of KBOs with well-determined orbits. Based on these classification works, an understanding of the importance of high-order resonances is emerging. Many objects that were thought to be scattering off Neptune are trapped in high-order resonance with that planet, perhaps indicating that Neptune's mean-motion resonance swept through an already excited Kuiper belt population (*Hahn and Malhotra,* 2005).

Murray-Clay and Chiang (2005) find that the structure of the 2:1 resonance may play a critical role in determining the timescales for Neptune's migration and conclude that the current population of 2:1 resonators excludes migration timescales shorter than ~10^6 yr. A careful mapping of the structure and populations of the various Kuiper belt resonances will provide many clues to the history of planet formation and evolution in this region. At this time, unfortunately, no strong constraints on the size and distribution of the 2:1 resonance is available. This is an area where future observational work would be fruitful. Unfortunately, the CFEPS projects L3 + Pre-Survey sample contains only one (or perhaps two) 2:1 resonant objects and very few constraints can be placed on this population at this time.

3.2.8. The scattering and detached objects. *Trujillo et al.* (2000) provide an estimate of the size of the "scattering" disk population. Based on their four initial detections, Trujillo et al. conclude that the underlying scattering population must be substantial, likely as large as the classical Kuiper belt population. This conclusion is based on the straightforward observation that scattered disk objects (SDOs) spend only a small fraction of their orbital period in the 30–50-AU zone where they can be detected, and therefore the discovery of four such objects indicates a relatively large parent population. One of the four SDOs reported by Tru-jillo et al. has subsequently been found to be in resonance (see chapter by Gladman et al.), reducing the original estimate of *Trujillo et al.* (2000) by 25%.

Gladman et al.'s chapter reports that 59 of the 541 classifiable KBOs are in either the "scattering" or "detached" orbital class, indicating a rather substantial population of such objects. We do not report here a measure of this interesting population of objects using the two detached and two scattering objects in the CFEPS L3 sample, as our estimates are extremely model dependent. We do note, however, that a large population (at least as large as that of classical belt) of SDOs with pericenters between 36 and 38 AU and semimajor axes extending out to hundreds of AU is consistent with all currently available observations.

4. SUMMARY

Many of the bulk properties of the Kuiper belt are now coming fully to light. Figure 4 provides a good visual representation of the emerging view of the Kuiper belt:

1. The "cold classical" Kuiper belt is a low-i, low-e component tucked into the 42.5 < a < 44.5-AU zone. This very "cold" component represents about 35% of the classical Kuiper belt population. Models where the cold belt extends beyond 45 AU are rejected.

2. The "hot classical" Kuiper belt contains a population of objects weighted toward large e ($P(e) \propto e$) and drawn from a broad inclination distribution that is well-represented by a Gaussian of width ~15°. This "hot" belt appears to uniformly fill the stable orbital phase-space between 35 and 47 AU and the detached objects *may* be the smooth extension of this population to larger a. The "hot" population represents about 65% of the classical Kuiper belt.

3. Many KBOs are trapped in (very) high-order mean-motion resonances with Neptune. Some of these high-order resonators have been mistakenly thought of as "scattered disk" objects. Clearly these high-order resonators provide an important clue to the evolution of the outer solar system. About 10% (open circles in Fig. 4) of the observed CFEPS sample is in this class.

4. The scattering and detached objects, although losing members to more accurate classification, continue to indicate that a substantial population of KBOs must reside in these populations. The debiased distance distribution of scattered objects is flat, indicating a shallow radial dependence (~r^{-1}) in this population. The detached population *may* be seen as a continuation of the hot classical KBOs beyond a ~ 50 AU.

We have demonstrated the strength of utilizing the CFEPS survey simulator to interpret models of the Kuiper belt's underlying populations. Future Kuiper belt surveys that provide such simulators will provide greatly enhanced constraints on the detailed structure of this region of the solar system.

REFERENCES

Allen R. L., Bernstein G. M., and Malhotra R. (2001) The edge of the solar system. *Astrophys. J. Lett., 549,* L241–L244.

Allen R. L., Bernstein G. M., and Malhotra R. (2002) Observational limits on a distant cold Kuiper belt. *Astron. J., 124,* 2949–2954.

Allen R. L., Gladman B., Kavelaars J. J., Petit J.-M., Parker J. W., and Nicholson P. (2006) Discovery of a low-eccentricity, high-inclination Kuiper belt object at 58 AU. *Astrophys. J. Lett., 640,* L83–L86.

Bernstein G. and Khushalani B. (2000) Orbit fitting and uncertainties for Kuiper belt objects. *Astron. J., 120,* 3323–3332.

Bernstein G. M., Trilling D. E., Allen R. L., Brown M. E., Holman M., and Malhotra R. (2004) The size distribution of trans-neptunian bodies. *Astron. J., 128,* 1364–1390.

Brown M. E. (2001) The inclination distribution of the Kuiper belt. *Astron. J., 121,* 2804–2814.

Brown M. E., Trujillo C., and Rabinowitz D. (2004) Discovery of a candidate inner Oort cloud planetoid. *Astrophys. J., 617,* 645–649.

Brown M. E., Trujillo C. A., and Rabinowitz D. L. (2005) Discovery of a planetary-sized object in the scattered Kuiper belt. *Astrophys. J. Lett., 635,* L97–L100.

Brown M. J. I. and Webster R. L. (1998) A search for bright Kuiper Belt objects. *Publ. Astron. Soc. Australia, 15,* 176–178.

Chiang E. I. and Brown M. E. (1999) Keck pencil-beam survey for faint Kuiper belt objects. *Astron. J., 118,* 1411–1422.

Chiang E. I., Lovering J. R., Millis R. L., Buie M. W., Wasserman L. H., and Meech K. J. (2003a) Resonant and secular families of the Kuiper belt. *Earth Moon Planets, 92,* 49–62.

Chiang E. I., Jordan A. B., Millis R. L., Buie M. W., Wasserman L. H., Elliot J. L., Kern S. D., Trilling D. E., Meech K. J., and Wagner R. M. (2003b) Resonance occupation in the Kuiper belt: Case examples of the 5:2 and Trojan resonances. *Astron. J., 126,* 430–443.

Dones L. (1997) Origin and evolution of the Kuiper belt. In *From Stardust to Planetesimals* (Y. J. Pendleton and A. G. G. M. Tielens, eds.), p. 347. ASP Conf. Series 122, San Francisco.

Duncan M. J. and Levison H. F. (1997) A scattered comet disk and the origin of Jupiter family comets. *Science, 276,* 1670–1672.

Elliot J. L. and 10 colleagues (2005) The Deep Ecliptic Survey: A search for Kuiper belt objects and Centaurs. II. Dynamical classification, the Kuiper belt plane, and the core population. *Astron. J., 129,* 1117–1162.

Gladman B., Kavelaars J. J., Nicholson P. D., Loredo T. J., and Burns J. A. (1998) Pencil-beam surveys for faint trans-neptunian objects. *Astron. J., 116,* 2042–2054.

Gladman B., Kavelaars J. J., Petit J.-M., Morbidelli A., Holman M. J., and Loredo T. (2001) The structure of the Kuiper belt: Size distribution and radial extent. *Astron. J., 122,* 1051–1066.

Gladman B., Holman M., Grav T., Kavelaars J., Nicholson P., Aksnes K., and Petit J.-M. (2002) Evidence for an extended scattered disk. *Icarus, 157,* 269–279.

Hahn J. M. and Malhotra R. (2005) Neptune's migration into a stirred-up Kuiper belt: A detailed comparison of simulations to observations. *Astron. J., 130,* 2392–2414.

Irwin M., Tremaine S., and Zytkow A. N. (1995) A search for slow-moving objects and the luminosity function of the Kuiper belt. *Astron. J., 110,* 3082.

Ivezić Ž. and 32 colleagues (2001) Solar system objects observed in the Sloan Digital Sky Survey commissioning data. *Astron. J., 122,* 2749–2784.

Jewitt D., Luu J., and Marsden B. G. (1992) 1992 QB1. *IAU Circular 5611,* 1.

Jewitt D., Luu J., and Marsden B. G. (1993) 1993 RO. *IAU Circular 5865,* 1.

Jewitt D., Luu J., and Chen J. (1996) The Mauna Kea-Cerro-Tololo (MKCT) Kuiper belt and Centaur survey. *Astron. J., 112,* 1225.

Jewitt D., Luu J., and Trujillo C. (1998) Large Kuiper belt objects: The Mauna Kea 8K CCD survey. *Astron. J., 115,* 2125–2135.

Jones R. L. and 16 colleagues (2006) The CFEPS Kuiper belt survey: Strategy and presurvey results. *Icarus, 185,* 508–522.

Kavelaars J. J., Jones L., Gladman B., Petit J., Parker J., and the CFEPS Team (2006) CFEPS [Canada-France Ecliptic Plane Survey]: The details. *AAS/Division for Planetary Sciences Meeting Abstracts, 38,* #44.02.

Larsen J. A., Gleason A. E., Danzl N. M., Descour A. S., McMillan R. S., Gehrels T., Jedicke R., Montani J. L., and Scotti J. V. (2001) The Spacewatch wide-area survey for bright Centaurs and trans-neptunian objects. *Astron. J., 121,* 562–579.

Liller W. (1993) Possible nova in Lupus. *IAU Circular 5867,* 2.

Luu J. X. and Jewitt D. C. (1998) Deep imaging of the Kuiper belt with the Keck 10 meter telescope. *Astrophys. J. Lett., 502,* L91.

Luu J., Jewitt D., and Marsden B. G. (1993) 1993 FW. *IAU Circular 5730,* 1.

Luu J.-X., Marsden B. G., Jewitt D., Truijillo C. A., Hergenrother C. W., Chen J., and Offutt W. B. (1997) A new dynamical class in the trans-neptunian solar system. *Nature, 387,* 573–575.

Lykawka P. S. and Mukai T. (2007) Origin of scattered disk resonant TNOs: Evidence for an ancient excited Kuiper belt of 50 AU radius. *Icarus, 186,* 331–341.

Malhotra R. (1993) The origin of Pluto's peculiar orbit. *Nature, 365,* 819.

Marsden B. G. (1994) 1993 RO, 1993 RP, 1993 SB, 1993 SC. *IAU Circular 5985,* 1.

Murray-Clay R. A. and Chiang E. I. (2005) A signature of planetary migration: The origin of asymmetric capture in the 2:1 resonance. *Astrophys. J., 619,* 623–638.

Petit J.-M., Holman M. J., Gladman B. J., Kavelaars J. J., Scholl H., and Loredo T. J. (2006a) The Kuiper belt luminosity function from m_R = 22 to 25. *Mon. Not. R. Astron. Soc., 365,* 429–438.

Petit J.-M., Gladman B., Kavelaars J. J., Jones R. L., Parker J., and Bieryla A. (2006b) The Canada-France Ecliptic Plane Survey: First (L3) data release. *AAS/Division for Planetary Sciences Meeting Abstracts, 38,* #44.01.

Sheppard S. S., Jewitt D. C., Trujillo C. A., Brown M. J. I., and Ashley M. C. B. (2000) A wide-field CCD survey for Centaurs and Kuiper belt objects. *Astron. J., 120,* 2687–2694.

Tholen D. J., Senay M., Hainaut O., and Marsden B. G. (1994) 1993 RO, 1993 RP, 1993 SB, 1993 SC. *IAU Circular 5983,* 1.

Tombaugh C. W. (1961) The trans-neptunian planet search. In *Planets and Satellites* (G. Kuiper and B. Middlehurst, eds.), p. 12. Univ. of Chicago, Chicago.

Trujillo C. A. and Brown M. E. (2001) The radial distribution of the Kuiper belt. *Astrophys. J. Lett., 554,* L95–L98.

Trujillo C. A. and Brown M. E. (2003) The Caltech wide area sky survey. *Earth Moon Planets, 92,* 99–112.

Trujillo C. and Jewitt D. (1998) A semiautomated sky survey for slow-moving objects suitable for a Pluto Express mission encounter. *Astron. J., 115,* 1680–1687.

Trujillo C. A., Jewitt D. C., and Luu J. X. (2000) Population of the scattered Kuiper belt. *Astrophys. J. Lett., 529,* L103–L106.

Trujillo C. A., Luu J. X., Bosh A. S., and Elliot J. L. (2001a) Large bodies in the Kuiper belt. *Astron. J., 122,* 2740–2748.

Trujillo C. A., Jewitt D. C., and Luu J. X. (2001b) Properties of the trans-neptunian belt: Statistics from the Canada-France-Hawaii Telescope survey. *Astron. J., 122,* 457–473.

Williams I. P., Fitzsimmons A., and O'Ceallaigh D. (1993) 1993 SB and 1993 SC. *IAU Circular 5869,* 1.